ACS APPLIED MATERIALS & INTERFACES

Research Article

www.acsami.org

[6,6]-Phenyl-C_{61}-butyric Acid 2-((2-(Dimethylamino)ethyl)(methyl)amino)-ethyl Ester as an Acceptor and Cathode Interfacial Material in Polymer Solar Cells

Menglan Lv,[†,‡,§,∥] Ming Lei,[†,⊥] Jin Zhu,[§] Tadahiko Hirai,[‡] and Xiwen Chen*[,‡]

[‡]Materials Science and Engineering, Commonwealth Scientific and Industrial Research Organisation (CSIRO), Clayton, Victoria 3168, Australia

[§]Chengdu Institute of Organic Chemistry, Chinese Academy of Sciences (CAS), Chengdu, Sichuan 610041, People's Republic of China

[∥]University of Chinese Academy of Sciences, Beijing, 100049, People's Republic of China

[⊥]Department of Chemistry, Zhejiang University, Hangzhou, Zhejiang 310027 People's Republic of China

Supporting Information

ABSTRACT: An amine-based, alcohol-soluble fullerene [6,6]-phenyl-C_{61}-butyric acid 2-((2-(dimethylamino)ethyl)(methyl)-amino)-ethyl ester (PCBDAN) with 4-fold electron mobility of 6,6-phenyl-C_{61}-butyric acid methyl ester (PCBM) is applied successfully as an acceptor and cathode interfacial material in polymer solar cells ITO/P3HT:PCBDAN/MoO_3/Ag, where indium tin oxide (ITO) alone is used as the cathode and poly(3-hexylthiophene) (P3HT) is used as a donor. The X-ray photoelectron spectroscopy (XPS) depth profile confirming a favorable vertical phase separation is formed where P3HT is rich at the air/active blend interface and PCBDAN is rich at the buried interface with ITO and, thus, reduces the work function of ITO for use as the cathode. A moderate power conversion efficiency (PCE) of 3.1% is achieved. The slightly low PCE could be due to unoptimized morphology and low structure ordering of P3HT in the blends. However, this result demonstrates that the amine-based fullerene could be used as the acceptor and cathode interfacial material, which eliminated the multilayer device fabrication process. Because PCBDAN has high electron mobility, it would have potential applications in nano-structured organic solar cells. In the near future, alcohol-processable, high-efficient organic/polymer solar cells can be anticipated.

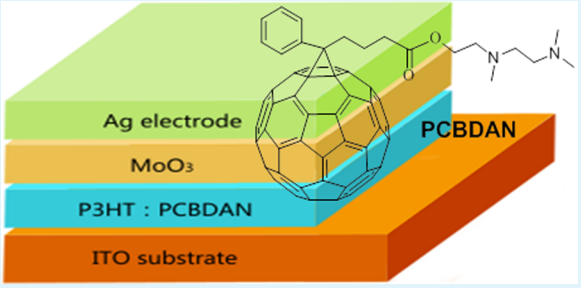

KEYWORDS: *fullerenes, photovoltaic devices, organic electronics, conjugated polymers, solar cells*

INTRODUCTION

Bulk-heterojunction polymer solar cells (PSCs) have attracted great interests, owing to the characteristics of low-cost, high-throughput, flexible, lightweight, and inexhaustible solar energy.[1] Recently, the power conversion efficiency (PCE) already reached 8.37[2] and 9.35%[3] for conventional and inverted single heterojunction PSCs, respectively, and 10.6% for tandem solar cells.[4] This progress has been mainly ascribed to application/modification of cathode interlayers and device architectures.[2−23] The most common cathode interfacial materials include inorganic oxide ZnO or its derivatives,[2−4] TiO_x,[5] alcohol/water-soluble conjugated polymers, such as polyfluorene derivatives with amino groups or ammonium salts[6−13] and grafted with K^+ intercalated crown ethers,[14] a hyperbranched conjugated polymer,[15] and insulating polymers with amine groups.[16] For a good cathode buffer layer, it needs to reduce the work function of cathodes to form ohmic contact between active layers and the cathodes and to have high electron mobility for efficient electron collection. Considering their n-type semiconductor character, high electron mobility, and good energy level matching with fullerene acceptors, such as 6,6-phenyl-C_{61}-butyric acid methyl ester (PCBM) used in active layers of PSCs, fullerene derivatives have been extensively employed recently as cathode interfacial materials, including self n-doped conducting fullerenes,[17,18] phosphate-based fullerene,[19] and amino- or ammonium-based fullerenes.[20−23]

The state-of-the-art PSC photoactive materials are mostly soluble in aromatic organic solvents, such as toluene, chlorobenzene, and 1,2-dichlorobenzene. Considering sustainability for industrial manufacturing, use of these toxic organic solvents will be harmful to the environment and the health of humans. It is thus important to develop environmentally friendly solvents, materials, and fabrication processes. Efforts have been made on developing water-soluble conjugated

Received: February 1, 2014
Accepted: March 24, 2014
Published: March 24, 2014

   dx.doi.org/10.1021/am5007047 | ACS Appl. Mater. Interfaces 2014, 6, 5844−5851

polymers or water-processable materials for applications, such as light-emitting diodes and solar cells.[24,25] For solar cell applications, a layer-by-layer approach with charged donors and fullerenes may suffer from short exciton diffusion lengths and possible p-doping of donors and n-doping of fullerenes, while aqueous dispersions of hydrophobic materials usually result in larger nanoparticle sizes.[18,26−30] Green-solvent-soluble fullerenes and semiconducting polymers including those alcohol- or ethyl-acetate-soluble fullerene derivatives and polymers have been reported.[17−23,31,32] However, solar cells based on these materials as donors or acceptors have not been realized thus far.

It was reported that amine-containing donors and acceptors were not working in conventional PSCs.[23] However, we demonstrated that an alcohol-soluble amine-modified fullerene derivative [6,6]-phenyl-C_{61}-butyric acid 2-((2-(dimethylamino)ethyl)(methyl) amino)-ethyl ester (PCBDAN) can be used as an additive in a donor−acceptor blend as cathode interfacial material.[22] The reason is that it self-organizes into a vertical phase-separated morphology[33,34] in favor of inverted device architecture, where PCBDAN was rich at the buried interface with indium tin oxide (ITO), serving as a cathode interfacial material reducing the work function of ITO for its direct use as the cathode.

In this paper, we successfully apply PCBDAN as an acceptor and cathode interfacial material in PSCs to give a PCE of 3.1%. PCBDAN can be dissolved at 5.0 mg/mL in methanol in the presence of a small amount of acetic acid. However, because we do not have suitable alcohol-soluble donors at the moment, we use a typical poly(3-hexylthiophene) (P3HT) as the donor for proof-of-concept. Therefore, a non-polar solvent 1,2-dichlorobenzene is used as the processing solvent for the photoactive blend. By X-ray photoelectron spectroscopy (XPS) analysis, surface energy measurements, and device characteristics, vertical phase separation in the present device is confirmed; PCBDAN is rich at the buried ITO interface, making ITO suitable as a cathode directly with reduced work function, where P3HT is rich at the air interface with MoO_3/Ag. This finding would be helpful for understanding the charge transport property in amine-containing materials and would lead to rapid development in alcohol-processable PSCs in the future.

RESULTS AND DISCUSSION

To evaluate the potential of PCBDAN as an acceptor, the energy level and electron mobility were measured. The highest occupied molecular orbital (HOMO) level of PCBDAN was measured by photoelectron spectroscopy in air (PESA) at 5.84 eV (see Figure S1 of the Supporting Information), and the optical band gap was measured from the onset of ultraviolet (UV) absorption at 2.2 eV (see Figure S2 of the Supporting Information); thus, the lowest unoccupied molecular orbital (LUMO) is calculated as −3.64 eV. In comparison, PCBM possesses the HOMO at 5.80 eV and the LUMO at 3.60 eV by the same methods (see Figures S1 and S2 of the Supporting Information). The small discrepancy between our values and literature data for PCBM (HOMO, 5.91 eV; LUMO, 3.91 eV)[35] may be due to different measurement methods. The amino group on the fullerene did not affect the energy levels of the fullerene, which is in good agreement with a recent report that amino-modified fullerene $PC_{71}BM$−N has a similar energy level to $PC_{71}BM$.[23]

The electron mobility of PCBDAN was estimated using the space-charge limited current (SCLC) method.[36] The electron-only devices ITO/PCBDAN (100 nm)/Al (100 nm) was used. Here, ITO alone was used as an electron collection electrode because PCBDAN can reduce its work function.[22] For comparison, the electron mobility of PCBM was also measured with electron-only device ITO/TIPD (12 nm)/PCBM (100 nm)/Al (100 nm), where TIPD represents a titanium chelate, which was used for the electron collection layer.[37] J−V characteristics of the single-carrier devices were shown in

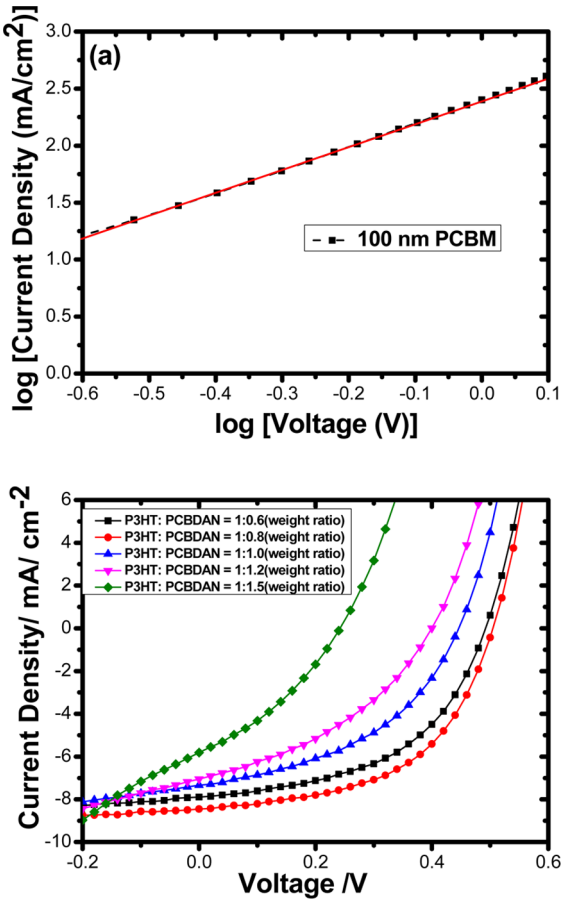

Figure 1. Current density versus applied voltage (J−V) characteristics of electron-only devices and the corresponding fitting results from the SCLC model (black line, measured; red line, fitted): (a) ITO/TIPD (12 nm)/PCBM (100 nm)/Al (100 nm) and (b) ITO/PCBDAN(100 nm)/Al (100 nm).

Figure 1, and the mobilities were calculated by fitting to the Mott−Gurney law,[36] which is expressed by

$$J = 9\varepsilon_r\varepsilon_0\mu V^2/8L^3 \quad (1)$$

where $\varepsilon_r\varepsilon_0$ is the dielectric constant of the material, L is the thickness of the active layer, and μ is the mobility.[36] The dielectric constants were calculated from the capacitance versus frequency measurement with impedance spectroscopy (see Figure S3 of the Supporting Information).[38] The dielectric constant of PCBM is 4.01, which is similar to the literature value (3.90),[39] and that of PCBDAN is 3.06. Under the SCLC, we fitted the experimental J−V data to eq 1 to obtain a slope of 2 in the logarithmical scales. The electron mobilities of PCBM and PCBDAN were calculated to be 6.31×10^{-4} and 2.92×10^{-3} $cm^2\ V^{-1}\ s^{-1}$, respectively. The fact that PCBDAN has a 4-fold electron mobility of PCBM is a good sign for PCBDAN as

dx.doi.org/10.1021/am5007047 | ACS Appl. Mater. Interfaces 2014, 6, 5844−5851

a potential good acceptor for PSCs and probably one of the reasons for it as a good cathode interfacial material.[20−22]

Recently, we demonstrated that PCBDAN could reduce the work function of ITO from 4.70 to 4.1 eV, and the work function of evaporated MoO_3 on PCBDAN film still remained high above 5.33 eV.[22] Therefore, inverted solar cells ITO/P3HT:PCBDAN/MoO_3/Ag were fabricated and tested. Here, ITO was used as the cathode, MoO_3/Ag was used as the anode, and P3HT, a typical and most studied polymer, was used as the donor, as shown in Chart 1. A control device ITO/P3HT:PCBM/MoO_3/Ag performed poor with a PCE of 0.30%, as reported previously.[22] In the presence of PCBDAN, the inverted devices worked reasonable well. The extracted device performance data from current−voltage characteristics in Figure 2 are shown in Table 1. A PCE of 3.06% was achieved with an open circuit voltage (V_{oc}) of 0.55 V, short circuit current (J_{sc}) of 9.41 mA/m^2, and fill factor (FF) of 59.1%. A slightly lower PCE of 2.77% was obtained from devices with an additional ZnO layer on top of ITO. No improvement with the typical electron collection layer ZnO means that the ITO cathode may already be modified by PCBDAN and, thus, possesses low work function for efficient electron collection. The PCE of 3.06% with PCBDAN as the acceptor, however, is slightly lower than a typical inverted device with PCBM as an acceptor, which gave a PCE of 3.49%. The morphology may play an important role as will be discussed below. From the above results, a schematic energy level diagram of the components within the inverted devices could be drawn, as in Chart 2.

Chart 1. Inverted Polymer Solar Cells and Molecule Structure of PCBDAN

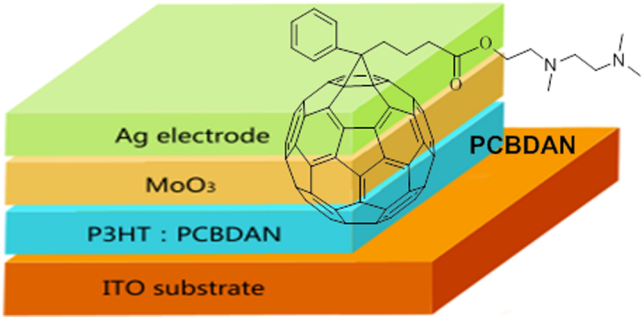

The formation of favorable vertical phase separation could be illustrated by XPS and contact angle measurements. The XPS combined with argon ion etching was carried out to analyze the surface atomic ratios (Table 2) and compositional depth profile from the air interface through to the buried blend/ITO interface for the sample without MoO_3/Ag (Figure 3). For the P3HT:PCBDAN blend, the surface S/C atomic ratio is 0.065, between 0.050 for the calculated ratio in the blend solution and 0.081 for the measured ratio for the pure P3HT film (the calculated ratio is 0.100). In addition, the surface N/C and O/C atomic ratios of 0.005 were obviously lower than the calculated value of 0.013 in the blend (Table 2). The results clearly showed that P3HT was rich at the top surface, while PCBDAN was poor. The composition depth profile in Figure 3 showed that the nitrogen and oxygen concentrations appeared to be increasing with depth. In addition, the sulfur concentration emerged with the opposite trend: the lowest value came out at the buried blend/ITO interface. The S/C ratio decreased rapidly from 0.065 to around 0.035 with the etching time, indicating that the top capping layer was very thin and the underneath part was close to the bulk properties (calculated S/C ratio for the blend is 0.050). The N/C atomic ratio reached 0.015, which is higher than 0.013 for the calculated blend but lower than 0.026 for the pure PCBDAN film (Table 2). Therefore, we can conclude that PCBDAN was rich at the buried interface with ITO, but no evidence was found for monolayer formation at this interface from the XPS measurement.

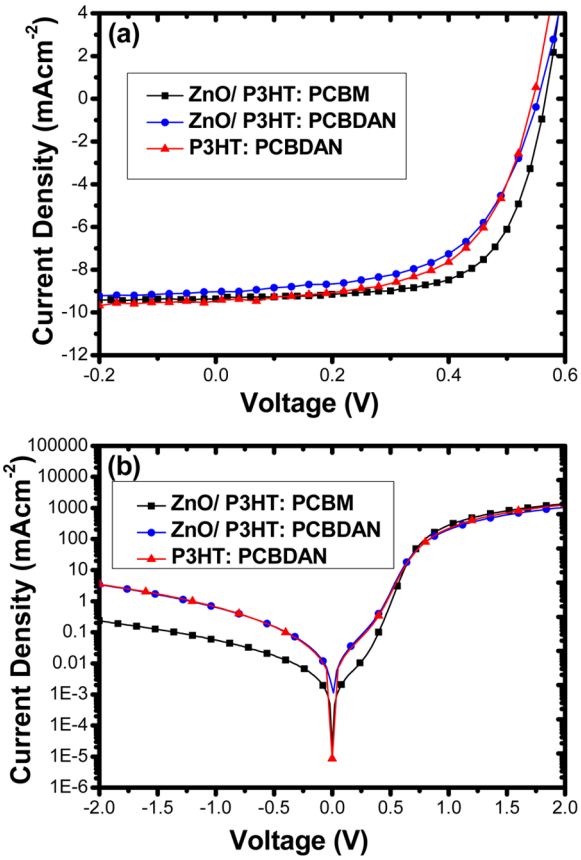

Figure 2. Current density−voltage (J−V) characteristics of the devices (a) under 1000 W/m^2 at AM1.5G illumination and (b) dark.

Evidence of the vertical phase separation has also been found with contact angle measurements.[40] The details for the measurement and method are in the Supporting Information. The contact angles and calculated surface energies of the ITO substrate and individual films on ITO substrates are shown in Table 3. The surface energy of the P3HT−PCBDAN blend (23.6 mN m^{-1}) was the same as that of P3HT (23.9 mN m^{-1}) within the experimental error. The surface energy components, γ^{LW}, attributed to Lifshitz−van der Waals interactions, γ^{AB}, attributed to acid−base interactions, and γ^-, the electron donor component, were also very similar to each other. This may indicate that the air interface was almost capped with a pure thin P3HT layer. A thin P3HT capping layer was found before by near-edge X-ray absorption fine structure spectroscopy (NEXAFS), ultraviolet photoemission spectroscopy (UPS), and angle-resolved XPS in the P3HT:PCBM blend[34,41−43] A similar phenomenon has been found in a ternary blend P3HT:PCBM:PCBDAN before.[22] The surface energy of the PCBDAN (30.4 mN m^{-1}) film was closer to that of ITO (40.0 mN m^{-1}) and higher than those of the P3HT film and P3HT−

dx.doi.org/10.1021/am5007047 | ACS Appl. Mater. Interfaces 2014, 6, 5844−5851

Table 1. Performance Data of Various PSCs Measured under 1000 W/m^2 at AM1.5G Illumination[a]

device	V_{oc} (V)	J_{sc} (mA cm^{-2})	FF (%)	PCE (%)	average PCE (%) (six devices)	R_s[b] (Ω cm^2)	R_{sh}[c] (kΩ cm^2)
A	0.56	9.37	66.6	3.49	3.40	7.63	1.04
B	0.55	9.02	58.5	2.90	2.77	8.22	1.09
C	0.55	9.41	59.1	3.06	3.01	8.22	1.09

[a]Device A, ITO/ZnO/P3HT:PCBM/MoO_3/Ag; device B, ITO/ZnO/P3HT:PCBDAN/MoO_3/Ag; and device C, ITO/P3HT:PCBDAN/MoO_3/Ag. [b]Series resistance R_s was measured from the slope under dark currents at 2.0 V. [c]Shunt resistance R_{sh} was measured from the slope under dark currents at the voltage where the current is at a minimum.

Chart 2. Energy Level Diagram Showing the HOMO and LUMO Energies of Each Component Material

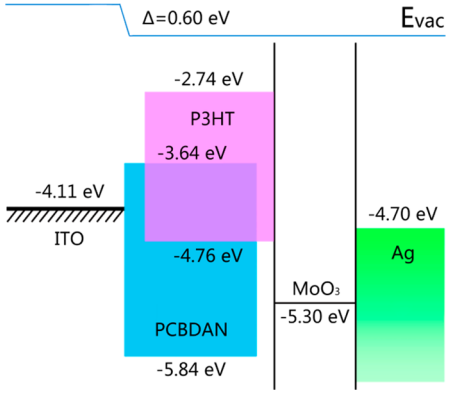

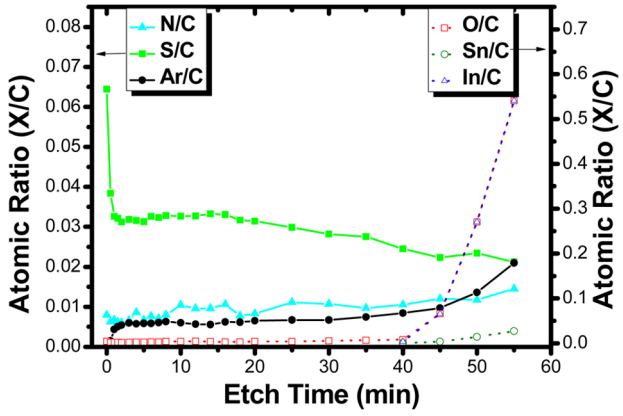

Figure 3. Element depth profile with Ar^+ sputtering time measured by XPS.

PCBDAN. In addition, the surface energy components of PCBDAN had similar values to that of ITO but significantly higher than those of P3HT and the blend film. The similar surface energy and the components for PCBDAN and ITO could be the driving force for PCBDAN to migrate toward the ITO substrate and form a PCBDAN-rich buried interface with ITO, characterized by thermodynamically stable composition profiles.[22,41]

To explore why the PCE of the device with PCBDAN is slightly lower than that with PCBM, the charge carrier mobilities were approximated using SCLC measurements of electron- and hole-only devices. Their device structures were ITO substrate/P3HT:PCBDAN (120 nm)/Al (100 nm) and ITO substrate/MoO_3 (10 nm)/P3HT:PCBDAN (120 nm)/MoO_3 (10 nm)/Ag (100 nm), respectively. The mobilities were calculated from the $J-V$ characteristics (Figure 4) by fitting to the Mott–Gurney law.[36] The electron mobility of 1.38×10^{-3} cm^2 V^{-1} s^{-1} is 267-fold the hole mobility (5.16×10^{-6} cm^2 V^{-1} s^{-1}). The good fitting for the hole-only device again confirmed that 10 nm of MoO_3 could work as the hole collection layer effectively, even in the presence of the amine-containing fullerene. The charge transport in the device was unbalanced, which may result in the buildup of space charges and charge recombination, which led to the lower efficiency. The unbalanced charge mobility may arise concern on space-charge limited photocurrent.[44] It was reported that an unbalanced charge mobility (ratio of electron and hole mobilities of 125) for an amorphous random co-poly(phenylene vinylene) blend with PCBM resulted in a space-charge limited photocurrent that set the device FF limit to 42%. However, photoactive blends of PCBM with different donor materials may have very different recombination loss mechanisms, and unbalanced charge mobility alone could not lead to a space-charge limited photocurrent for all blends.[45,46] Very recently, it was reported that the blend of poly[*N*-9″-heptadecanyl-2,7-carbazole-alt-5,5-(4′,7′-di-2-thienyl-2′,1′,3′-benzothiadiazole)] (PCDTBT):[6,6]-phenyl-C_{70}-butyric acid methyl ester ($PC_{70}BM$) at a 1:4 weight ratio has unbalanced charge mobility (electron and hole mobility ratio of 100) but gives a PCE over 6%, while a more balanced charge mobility at a 1:1 weight ratio gives a lower PCE of 2.2%.[47] Thus, the unbalanced charge mobility in the P3HT:PCBDAN blend may not result in a space-charge limited photocurrent, and a FF higher than 42% is reasonable.

To fine tune the morphology of the donor/acceptor blend films, we attempted to add solvent additives in the blend. A large bank of solvent additives was reported to improve PSC performance, including 1,8-octanedithiol,[48] 1,8-diiodooctane (DIO),[49] 1-chloronaphthalene,[50] *N*-methylpyrrolidone,[51] 3-methylthiophene (3MT),[52] *N*,*N*-dimethylformamide, and dimethyl sulfoxide.[53] Herein, we tested two different additives, DIO and 3MT. The former is a good solvent for PCBM, while the latter is a good solvent for P3HT. With the DIO additive, all parameters of the devices have become worse, with a lower PCE of 1.86%. In the case of 3MT, the device gave similar PCE

Table 2. Surface Atomic Ratios of Elements by XPS Analysis

	measured atomic ratio (X/C)				calculated atomic ratio (X/C)			
film	C/C	N/C	O/C	S/C	C/C	N/C	O/C	S/C
PCBDAN	1.00	0.026	0.026		1.00	0.026	0.026	
P3HT	1.00		0.003	0.081	1.00			0.100
P3HT:PCBDAN	1.00	0.005	0.005	0.065	1.00	0.013	0.013	0.050

dx.doi.org/10.1021/am5007047 | ACS Appl. Mater. Interfaces 2014, 6, 5844–5851

Table 3. Advancing Contact Angles of Three Probing Liquids on the Surfaces of ITO, ITO/PCBDAN, ITO/P3HT, and ITO/P3HT:PCBDAN (1:0.8 by w/w) at the Initial State and the Calculated Surface Energy (in mN/m)

		ITO	PCBDAN	P3HT	P3HT:PCBDAN
contact angle (deg)	water	14 ± 1	33 ± 3	107 ± 1	106 ± 1
	ethylene glycol	27 ± 2	45 ± 3	79 ± 1	80 ± 1
	hexydecane	15 ± 1	15 ± 1	31 ± 1	32 ± 1
calculated surface energy component (mN/m)	γ	40.0	30.4	23.9	23.6
	γ^{LW}	26.4	26.4	23.8	23.4
	γ^{AB}	13.7	4.04	0.14	0.14
	γ^{+}	0.62	0.06	0.08	0.12
	γ^{-}	75.0	68.1	0.07	0.16

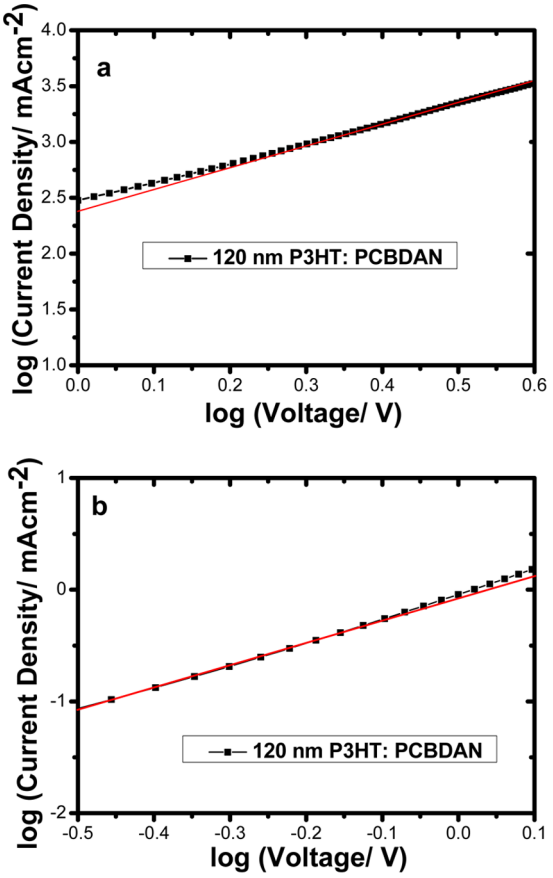

Figure 4. Measured current density versus applied voltage (J–V) characteristics of (a) electron-only device ITO substrate/P3HT:PCBDAN (120 nm)/Al (100 nm) and (b) hole-only device ITO/MoO_3 (10 nm)/P3HT:PCBDAN (120 nm)/MoO_3 (10 nm)/Ag (100 nm). Black line, measured; red line, fitted.

to the device without an additive but slightly different V_{oc} and J_{sc} (Table 4).

To understand how the additives affect the device performance, ultraviolet–visible (UV–vis) spectroscopy and atomic force microscopy (AFM) were conducted and the results are shown in Figures 5 and 6 and Table 5. For comparison, the

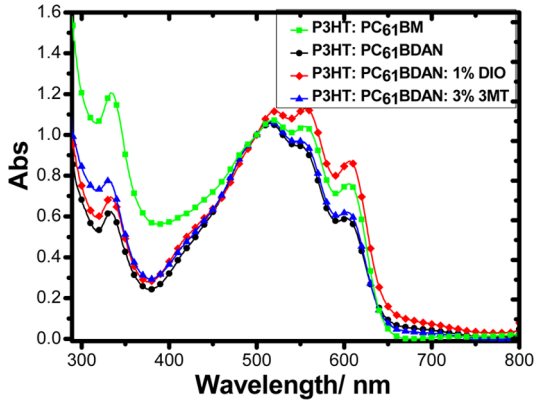

Figure 5. Absorption spectra of the blend films of P3HT:PCBM (1:1, w/w) and P3HT:PCBDAN (1:0.8, w/w) with or without additives.

results on the P3HT:PCBM film are also included. The addition of DIO made the UV–vis vibronic transition of P3HT at the long wavelength stronger than those in P3HT:PCBM and P3HT:PCBDAN films without an additive. This indicated the improved structure ordering of P3HT. However, the phase contrast [the root mean square (RMS) is 123.6°] and the domain size with the DIO additive may be bigger than the others (43.9° and 106.8°). The 3MT additive, on the other hand, resulted in similar vibronic peak intensity as in the blend without a solvent additive and did not bring the vibronic peak intensity up to the level in the P3HT:PCBM blend. This indicated that the structure ordering of P3HT was less than that in P3HT:PCBM. The electron mobility of the P3HT:PCBDAN blend was found to be half of that of pure PCBDAN, but the hole mobility of 5.16×10^{-6} cm^2 V^{-1} s^{-1} was quite low and comparable to the value for a unoptimized P3HT:PCBM blend.[54] Therefore, P3HT in its blend with PCBDAN has not

Table 4. Device Performance with Various Solvent Additives Measured under 1000 W/m^2 at AM1.5G Illumination for Device ITO/P3HT:PCBDAN/MoO_3/Ag

additive	V_{oc} (V)	J_{sc} (mA cm^{-2})	FF (%)	PCE (%)	average PCE (%) (six devices)	R_s[a] (Ω cm^2)	R_{sh}[b] (kΩ cm^2)
none	0.55	9.41	59.1	3.06	3.01	8.22	1.09
1.0% DIO	0.48	8.24	50.3	1.99	1.87	1.24	1.76
3.0% 3MT	0.52	9.89	58.5	3.01	2.96	1.18	1.59

[a]Series resistance R_s was measured from the slope under dark currents at 2.0 V. [b]Shunt resistance R_{sh} was measured from the slope under dark currents at the voltage where the current is a minimum.

dx.doi.org/10.1021/am5007047 | ACS Appl. Mater. Interfaces 2014, 6, 5844–5851

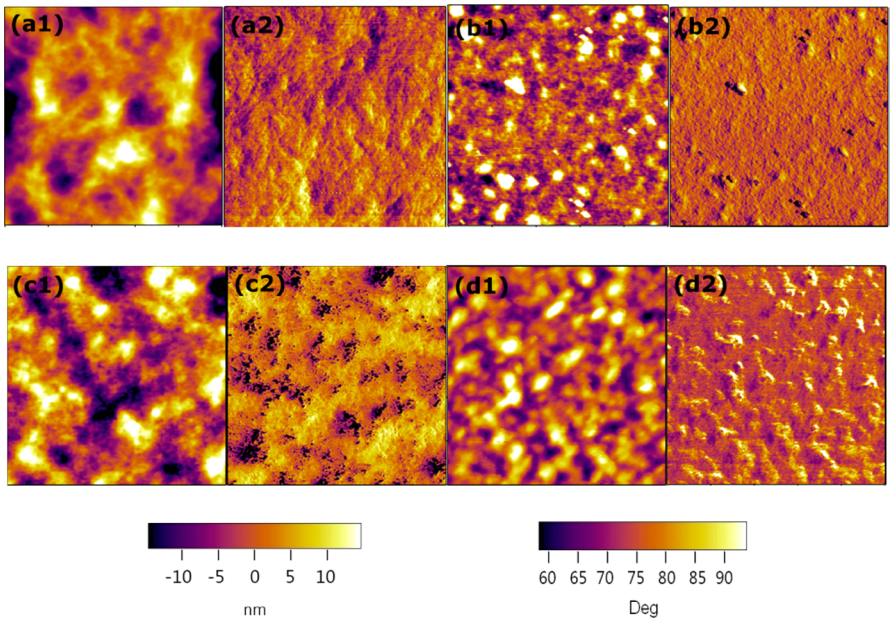

Figure 6. Surface topographies (1) and phase images (2) of the blend films of (a) P3HT:PCBM (1:1, w/w) and (b) P3HT:PCBDAN (1:0.8, w/w) without additives and with (c) 1.0% DIO and (d) 3.0% 3MT.

Table 5. Roughness Analysis of AFM

film	height RMS (nm)	phase RMS (deg)
ITO/ZnO/P3HT:PCBM	12.940	43.883
ITO/P3HT:PCBDAN	2.204	106.838
ITO/P3HT:PCBDAN (with 1.0% DIO)	6.751	123.647
ITO/P3HT:PCBDAN (with 3.0% 3MT)	5.902	76.252

formed comparable morphology or structure ordering as in its blend with PCBM. Further morphological tuning and more detailed studies on the relationship of the device performance with optoelectronic properties are needed for a more clear understanding of this point.

CONCLUSION

An amine-modified fullerene PCBDAN was successfully used as an acceptor and cathode interfacial material in PSCs ITO/P3HT:PCBDAN/MoO_3/Ag. Vertical phase separation in favor of the inverted device structure was confirmed by XPS depth profile, contact angle measurement, and device characteristics. PCBDAN was rich at the buried interface with ITO and reduced the work function of ITO, so that a simple device with ITO alone as the cathode worked, where a cathode interfacial layer, such as ZnO or other cathode interlayer, was not necessary. The elimination of a thin interlayer may have advantage for large area device fabrication. The reason for the driving force for the formation was that PCBDAN has a similar surface energy and its components to ITO but higher than P3HT. Because PCBDAN has 4-fold electron mobility of PCBM and the ability to reduce metal work functions, it may have potential applications in nano-structured organic solar cells as both an acceptor and a cathode interfacial material.[55−57] More importantly, charge transport properties of materials with amine moiety need re-evaluation under suitable device architectures for the SCLC method or field effect transistors to avoid a high hole injection barrier. Because the amine-modified materials could be alcohol-soluble and modification with amine moiety did not change the energy levels significantly, a green solvent, such as alcohol-processable, high-efficient organic/polymer solar cells, could be anticipated with alcohol-soluble donors and optimization of the donor−acceptor in the near future.

EXPERIMENTAL SECTION

Materials. All solvents were purchased from Sigma-Aldrich. P3HT and [6,6]-phenyl-C_{61} butyric acid methyl ester ($PC_{61}BM$) were purchased from Merck Chemical and Nano-C, Inc., respectively. The PCBDAN was synthesized in accordance with the literature method.[20]

Preparation of ZnO Films. ZnO nanoparticles were synthesized according to the literature.[58]

Device Fabrication. The solar cell device structures were ITO substrate/with or without ZnO/P3HT:PCBDAN (120 nm)/MoO_3(10 nm)/Ag (100 nm) and ITO substrate/ZnO (40 nm)/P3HT:PCBM (110 nm)/MoO_3(10 nm)/Ag (100 nm). ITO-coated glass substrates (Lumtec 5 Ω square^{-1}) were cleaned sequentially with detergent aqueous solution, deionized water, acetone, and isopropyl alcohol. The cleaned substrates were then exposed to UV ozone for 10 min at 30 °C (Novascan PDS-UVT). After that, the P3HT:PCBDAN (26 mg/mL, 1:0.8 ratio by weight) blend film was directly spin-coated onto the ITO substrates at 2800 rpm for 45 s inside a glove box filled with nitrogen and then thermally annealed at 120 °C for 10 min. In the case of ZnO, ZnO was spin-coated (4000 rpm for 30 s) on the treated ITO substrates and then annealed at 200 °C for 10 min in air. The P3HT:PCBM (15 mg/mL, 1:1 ratio by weight) blend active layer film was directly spin-coated onto the ZnO-treated substrates at 1300 rpm for 60 s inside the glove box. Finally, the devices were completed after deposition of 10 nm MoO_3 and 100 nm Ag (Kurt J. Lesker) as the electrode in a vacuum evaporator (Angstrom Engineering, Inc.) equipped with a variety of masks and a gradient shutter at a pressure below 2×10^{-6} Torr. The shadow masks gave the PSC device areas of 0.10 cm^2. In the case of single carrier devices, respective electrodes and MoO_3 have been thermally evaporated accordingly.

Measurements of *J*−*V* Characteristics. Current density−voltage (*J*−*V*) characteristics of the devices were measured with an Oriel solar simulator fitted with a 1000 W Xe lamp filtered to give an output of 1000 W/m^2 at AM1.5G. The xenon lamp was calibrated using a standard filtered silicon reference cell (Peccell Limited, Inc.). The

dx.doi.org/10.1021/am5007047 | ACS Appl. Mater. Interfaces 2014, 6, 5844−5851

devices were tested using a Keithley 2400 source meter controlled by Labview software.

Other Characterization Methods. The surface potentials were measured on a SKP5050 K probe system (KP Technology) in air. The work functions were achieved from an average value of 200 points for each sample. The roughness analysis and atomic force microscopy (AFM) images were carried out on a MFD-3D AFM instrument in AC mode with a NSC15/AIBS Si cantilever (resonant frequency around 325 kHz from μ-masch). The contact angles were measured with a CAM 200 (KSV Instrument, Ltd.). Ionization potentials of the films were measured by PESA on a Riken Keiki AC2 spectrometer with a light power of 10 nW and a power number of 0.5. UV−vis spectra were measured with a Cary 5E UV−vis−NIR spectrophotometer. Dielectric constant measurements were carried out with a Solartron SI-1255 and 1296 frequency response analyser system. The thickness of the active layer was measured with Dektak 6M stylus profiler (Veeco, Inc.). XPS analysis was performed using an AXIS Ultra DLD spectrometer (Kratos Analytical, Inc., Manchester, U.K.) with a monochromated Al Kγ source at a power of 150 W (15 kV × 10 mA), a hemispherical analyser operating in the fixed analyser transmission mode, and the standard aperture (analysis area of 0.3 × 0.7 mm). The total pressure in the main vacuum chamber during analysis was typically between 10^{-9} and 10^{-8} mbar.

■ ASSOCIATED CONTENT

Supporting Information

Ionization potential measurements, UV−vis absorption spectra, dielectric constant measurements, device optimizations, and calculation of the surface energy of various films. This material is available free of charge via the Internet at http://pubs.acs.org.

■ AUTHOR INFORMATION

Corresponding Author

*E-mail: xwchen5702@hotmail.com.

Author Contributions

[†]Menglan Lv and Ming Lei contributed equally to this work.

Notes

The authors declare no competing financial interest.

■ ACKNOWLEDGMENTS

This work was supported by CSIRO through a CAS−CSIRO joint project on the "Nanotechnology and Novel Energy Materials" focus area. The authors thank Dr. Thomas Gengenbach for XPS measurements.

■ REFERENCES

(1) Yu, G.; Gao, J.; Hummelen, J. C.; Wudl, F.; Heeger, A. J. Polymer photovoltaic cells: Enhanced efficiencies via a network of internal donor−acceptor heterojunctions. *Science* **1995**, *270*, 1789−1791.

(2) He, Z. C.; Zhong, C. M.; Huang, X.; Wong, W. Y.; Wu, H. B.; Chen, L. W.; Su, S. J.; Cao, Y. Simultaneous enhancement of open-circuit voltage, short-circuit current density, and fill factor in polymer solar cells. *Adv. Mater.* **2011**, *23*, 4636−4643.

(3) Liao, S. H.; Jhuo, H. J.; Cheng, Y. S.; Chen, S. A. Fullerene derivative-doped zinc oxide nanofilm as the cathode of inverted polymer solar cells with low-bandgap polymer (PTB7-Th) for high performance. *Adv. Mater.* **2013**, *25*, 4766−4771.

(4) You, J. B.; Dou, L. T.; Yoshimura, K.; Kato, T.; Ohya, K.; Moriarty, T.; Emery, K.; Chen, C. C.; Gao, J.; Li, G.; Yang, Y. A polymer tandem solar cell with 10.6% power conversion efficiency. *Nat. Commun.* **2013**, *4*, 1446.

(5) Kim, J. Y.; Lee, K.; Coates, N. E.; Moses, D.; Nguyen, T. Q.; Dante, M.; Heeger, A. J. Efficient tandem polymer solar cells fabricated by all-solution processing. *Science* **2007**, *317*, 222−226.

(6) Huang, F.; Hou, L. T.; Wu, H. B.; Wang, X. H.; Shen, H. L.; Cao, W.; Yang, W.; Cao, Y. High-efficiency, environment-friendly electroluminescent polymers with stable high work function metal as a cathode: Green- and yellow-emitting conjugated polyfluorene polyelectrolytes and their neutral precursors. *J. Am. Chem. Soc.* **2004**, *126*, 9845−9853.

(7) He, Z. C.; Zhong, C. M.; Su, S. J.; Xu, M.; Wu, H. B.; Cao, Y. Enhanced power-conversion efficiency in polymer solar cells using an inverted device structure. *Nat. Photonics* **2012**, *6*, 591−595.

(8) He, C.; Zhong, C.; Wu, H.; Yang, R.; Yang, W.; Huang, F.; Bazan, G. C.; Cao, Y. Origin of the enhanced open-circuit voltage in polymer solar cells via interfacial modification using conjugated polyelectrolytes. *J. Mater. Chem.* **2010**, *20*, 2617−2622.

(9) Huang, F.; Wu, H. B.; Cao, Y. Water/alcohol soluble conjugated polymers as highly efficient electron transporting/injection layer in optoelectronic devices. *Chem. Soc. Rev.* **2010**, *39*, 2500−2521.

(10) Liu, S. J.; Zhang, K.; Lu, J. M.; Zhang, J.; Yip, H. L.; Huang, F.; Cao, Y. High-efficiency polymer solar cells via the incorporation of an amino-functionalized conjugated metallopolymer as a cathode interlayer. *J. Am. Chem. Soc.* **2013**, *135*, 15326−15329.

(11) Chang, Y. M.; Zhu, R.; Richard, E.; Chen, C. C.; Li, G.; Yang, Y. Electrostatic self-assembly conjugated polyelectrolyte−surfactant complex as an interlayer for high performance polymer solar cells. *Adv. Funct. Mater.* **2012**, *22*, 3284−3289.

(12) Yang, T. B.; Wang, M.; Duan, C. H.; Hu, X. W.; Huang, L.; Peng, J. B.; Huang, F.; Gong, X. Inverted polymer solar cells with 8.4% efficiency by conjugated polyelectrolyte. *Energy Environ. Sci.* **2012**, *5*, 8208−8214.

(13) Jo, J.; Pouliot, J. R.; Wynands, D.; Collins, S. D.; Kim, J. Y.; Nguyen, T. L.; Woo, H. Y.; Sun, Y. M.; Leclerc, M.; Heeger, A. J. Enhanced efficiency of single and tandem organic solar cells incorporating a diketopyrrolopyrrole-based low-bandgap polymer by utilizing combined ZnO/polyelectrolyte electron-transport layers. *Adv. Mater.* **2013**, *25*, 4783−4788.

(14) Liao, S. H.; Li, Y. L.; Jen, T. H.; Cheng, Y. S.; Chen, S. A. Multiple functionalities of polyfluorene grafted with metal ion-intercalated crown ether as an electron transport layer for bulk-heterojunction polymer solar cells: Optical interference, hole blocking, interfacial dipole, and electron conduction. *J. Am. Chem. Soc.* **2012**, *134*, 14271−14274.

(15) Lv, M. L.; Li, S. S.; Jasieniak, J. J.; Hou, J. H.; Zhu, J.; Tan, Z. H.; Watkins, S. E.; Li, Y. F.; Chen, X. W. A hyperbranched conjugated polymer as the cathode interlayer for high-performance polymer solar cells. *Adv. Mater.* **2013**, *25*, 6889−6894.

(16) Zhou, Y. H.; Fuentes-Hernandez, C.; Shim, J.; Meyer, J.; Giordano, A. J.; Li, H.; Winget, P.; Papadopoulos, T.; Cheun, H.; Kim, J.; Fenoll, M.; Dindar, A.; Haske, W.; Najafabadi, E.; Khan, T. M.; Sojoudi, H.; Barlow, S.; Graham, S.; Brédas, J.; Marder, S. R.; Kahn, A.; Kippelen, B. A universal method to produce low-work function electrodes for organic electronics. *Science* **2012**, *336*, 327−332.

(17) O'Malley, K. M.; Li, C. Z.; Yip, H. L.; Jen, A. K.-Y. Enhanced open-circuit voltage in high performance polymer/fullerene bulk-heterojunction solar cells by cathode modification with a C_{60} surfactant. *Adv. Energy Mater.* **2012**, *2*, 82−86.

(18) Li, C. Z.; Chueh, C. C.; Yip, H. L.; Ding, F.; Li, X.; Jen, A. K.-Y. Solution-processible highly conducting fullerenes. *Adv. Mater.* **2013**, *25*, 2457−2461.

(19) Duan, C. H.; Zhong, C. M.; Liu, C. C.; Huang, F.; Cao, Y. Highly efficient inverted polymer solar cells based on an alcohol soluble fullerene derivative interfacial modification material. *Chem. Mater.* **2012**, *24*, 1682−1689.

(20) Li, S. S.; Lei, M.; Lv, M. L.; Watkins, S. E.; Tan, Z. A.; Zhu, J.; Hou, J. H.; Chen, X. W.; Li, Y. F. [6,6]-Phenyl-C_{61}-butyric acid dimethylamino ester as a cathode buffer layer for high-performance polymer solar cells. *Adv. Energy Mater.* **2013**, *23*, 1569−1574.

(21) Hong, D.; Lv, M. L.; Lei, M.; Chen, Y.; Lu, P.; Wang, Y. G.; Zhu, J.; Wang, H. Q.; Gao, M.; Watkins, S. E.; Chen, X. W. *N*-Acyldithieno[3,2-b:2′,3′-d]pyrrole-based low-band-gap conjugated polymer solar cells with amine-modified [6,6]-phenyl-C_{61}-butyric acid ester cathode interlayers. *ACS Appl. Mater. Interfaces* **2013**, *5*, 10995−11003.

(22) Ma, D.; Lv, M.; Lei, M.; Zhu, J.; Wang, H.; Chen, X. Self-organization of amine-based cathode interfacial materials in inverted polymer solar cells. *ACS Nano* **2014**, *8*, 1601−1608.
(23) Duan, C.; Cai, W.; Hsu, B. B. Y.; Zhong, C.; Zhang, K.; Liu, C.; Hu, Z.; Huang, F.; Bazan, G. C.; Heeger, A. J.; Cao, Y. Toward green solvent processable photovoltaic materials for polymer solar cells: The role of highly polar pendant groups in charge carrier transport and photovoltaic behavior. *Energy Environ. Sci.* **2013**, *6*, 3022−3034.
(24) Liu, B.; Yu, W. L.; Lai, Y. H.; Huang, W. Synthesis of a novel cationic water-soluble efficient blue photoluminescent conjugated polymer. *Chem. Commun.* **2000**, 551−552.
(25) Kietzke, T.; Neher, D.; Landfester, K.; Montenegro, R.; Guntner, R.; Scherf, U. Novel approaches to polymer blends based on polymer nanoparticles. *Nat. Mater.* **2003**, *2*, 408−412.
(26) Zhou, H.; Zhang, Y.; Mai, C.-K.; Collins, S. D.; Nguyen, T.-Q.; Bazan, G. C.; Heeger, A. J. Conductive conjugated polyelectrolyte as hole-transporting layer for organic bulk heterojunction solar cells. *Adv. Mater.* **2014**, *26*, 780−785.
(27) Mwaura, J. K.; Pinto, M. R.; Witker, D.; Ananthakrishnan, N.; Schanze, K. S.; Reynolds, J. R. Photovoltaic cells based on sequentially adsorbed multilayers of conjugated poly(*p*-phenylene ethynylene)s and a water-soluble fullerene derivative. *Langmuir* **2005**, *21*, 10119−10126.
(28) Taranekar, P.; Qiao, Q.; Jiang, H.; Ghiviriga, I.; Schanze, K. S.; Reynolds, J. R. Hyperbranched conjugated polyelectrolyte bilayers for solar-cell applications. *J. Am. Chem. Soc.* **2007**, *129*, 8958−8959.
(29) Andersen, T. R.; Larsen-Olsen, T. T.; Andreasen, B.; Bottiger, A. P. L.; Carle, J. E.; Helgesen, M.; Bundgaard, E.; Norrman, K.; Andreasen, J. W.; Jorgensen, M.; Krebs, F. C. Aqueous processing of low-band-gap polymer solar cells using roll-to-roll methods. *ACS Nano* **2011**, *5*, 4188−4196.
(30) Li, C. Z.; Chueh, C. C.; Ding, F. Z.; Yip, H. L.; Liang, P. W.; Li, X. S.; Jen, A. K. Y. Doping of fullerenes via anion-induced electron transfer and its implication for surfactant facilitated high performance polymer solar cells. *Adv. Mater.* **2013**, *25*, 4425−4430.
(31) Henson, Z. B.; Zhang, Y.; Nguyen, T. Q.; Seo, J. H.; Bazan, G. C. Synthesis and properties of two cationic narrow band gap conjugated polyelectrolytes. *J. Am. Chem. Soc.* **2013**, *135*, 4163−4166.
(32) Henson, Z. B.; Zalar, P.; Chen, X. F.; Welch, G. C.; Nguyen, T. Q.; Bazan, G. C. Towards environmentally friendly processing of molecular semiconductors. *J. Mater. Chem. A* **2013**, *1*, 11117−11120.
(33) Chen, L. M.; Hong, Z. R.; Li, G.; Yang, Y. Recent progress in polymer solar cells: Manipulation of polymer:fullerene morphology and the formation of efficient inverted polymer solar cells. *Adv. Mater.* **2009**, *21*, 1434−1449.
(34) Xu, Z.; Chen, L. M.; Yang, G. W.; Huang, C. H.; Hou, J. H.; Wu, Y.; Li, G.; Hsu, C. S.; Yang, Y. Vertical phase separation in poly(3-hexylthiophene):fullerene derivative blends and its advantage for inverted structure solar cells. *Adv. Funct. Mater.* **2009**, *19*, 1227−1234.
(35) He, Y. J.; Zhao, G. J.; Peng, B.; Li, Y. F. High-yield synthesis and electrochemical and photovoltaic properties of indene-C_{70} bisadduct. *Adv. Funct. Mater.* **2010**, *20*, 3383−3389.
(36) Blom, W. M.; Vissenberg, M. C. J. M. Charge transport in poly(*p*-phenylene vinylene) light-emitting diodes. *Mater. Sci. Eng.* **2000**, *27*, 53−94.
(37) Tan, Z. A.; Zhang, W.; Zhang, Z.; Qian, D.; Huang, Y.; Hou, J. H.; Li, Y. F. High-performance inverted polymer solar cells with solution-processed titanium chelate as electron-collecting layer on ITO electrode. *Adv. Mater.* **2012**, *24*, 1476−1481.
(38) Guo, M.; Hayakawa, T.; Kakimoto, M.; Goodson, T. Organic macromolecular high dielectric constant materials: Synthesis, characterization, and applications. *J. Phys. Chem. B* **2011**, *115*, 13419−13432.
(39) Mihailetchi, V. D.; Van Duren, J. K. J.; Blom, P. W. M.; Hummelen, J. C.; Janssen, R. A. J.; Kroon, J. M.; Rispens, M. T.; Verhees, W. J. H.; Wienk, M. M. Electron transport in a methanofullerene. *Adv. Funct. Mater.* **2003**, *13*, 43−46.
(40) Wang, X. J.; Ederth, T.; Inganäs, O. In situ Wilhelmy balance surface energy determination of poly(3-hexylthiophene) and poly(3,4-ethylenedioxythiophene) during electrochemical doping−dedoping. *Langmuir* **2006**, *22*, 9287−9294.
(41) Clark, M. D.; Jespersen, M. L.; Patel, R. J.; Leever, B. J. Predicting vertical phase segregation in polymer−fullerene bulk heterojunction solar cells by free energy analysis. *ACS Appl. Mater. Interfaces* **2013**, *5*, 4799−4807.
(42) Xue, B.; Vaughan, B.; Poh, C. −H.; Burke, K. B.; Thomsen, L.; Stapleton, A.; Zhou, X.; Bryant, G. W.; Belcher, W.; Dastoor, P. C. Vertical stratification and interfacial structure in P3HT:PCBM organic solar cells. *J. Phys. Chem. C* **2010**, *114*, 15797−15805.
(43) Vaynzof, Y.; Kabra, D.; Zhao, L.; Chua, L. L.; Steiner, U.; Friend, R. H. Surface-directed spinodal decomposition in poly[3-hexylthiophene] and C_{61}-butyric acid methyl ester blends. *ACS Nano* **2011**, *5*, 329−336.
(44) Mihailetchi, V. D.; Wildeman, J.; Blom, P. W. M. Space-charge limited photocurrent. *Phys. Rev. Lett.* **2005**, *94*, 126602.
(45) Andersson, L. M.; Muller, C.; Badada, B. H.; Zhang, F.; Wurfel, U.; Inganas, O. Mobility and fill factor correlation in geminate recombination limited solar cells. *J. Appl. Phys.* **2011**, *110*, 24509.
(46) Dibb, G. F. A.; Jamieson, F. C.; Maurano, A.; Nelson, J.; Durrant, J. R. Limits on the fill factor in organic photovoltaics: Distinguishing nongeminate and geminate recombination mechanisms. *J. Phys. Chem. Lett.* **2013**, *4*, 803−808.
(47) Armin, A.; Juska, C.; Ullah, M.; Velusamy, M.; Burn, P. L.; Meredith, P.; Pivrikas, A. Balanced carrier mobilities: Not a necessary condition for high-efficiency thin organic solar cells as determined by MIS-CELIV. *Adv. Energy Mater.* **2014**, DOI: 10.1002/aenm.201300954.
(48) Peet, J.; Kim, J. Y.; Coates, N. E.; Ma, W. L.; Moses, D.; Heeger, A. J.; Bazan, G. C. Efficiency enhancement in low-bandgap polymer solar cells by processing with alkane dithiols. *Nat. Mater.* **2007**, *6*, 497−500.
(49) Lee, J. K.; Ma, W. L.; Brabec, C. J.; Yuen, J.; Moon, J. S.; Kim, J. Y.; Lee, K.; Bazan, G. C.; Heeger, A. J. Processing additives for improved efficiency from bulk heterojunction solar cells. *J. Am. Chem. Soc.* **2008**, *130*, 3619−3623.
(50) Guo, X.; Cui, C. H.; Zhang, M. J.; Huo, L. J.; Huang, Y.; Hou, J. H.; Li, Y. F. High efficiency polymer solar cells based on poly(3-hexylthiophene)/indene−C_{70} bisadduct with solvent additive. *Energy Environ. Sci.* **2012**, *5*, 7943−7949.
(51) Yao, Y.; Hou, J. H.; Xu, Z.; Li, G.; Yang, Y. Effects of solvent mixtures on the nanoscale phase separation in polymer solar cells. *Adv. Funct. Mater.* **2008**, *18*, 1783−1789.
(52) Sun, Y. P.; Cui, C. H.; Wang, H. Q.; Li, Y. F. Efficiency enhancement of polymer solar cells based on poly(3-hexylthiophene)/indene−C_{70} bisadduct via methylthiophene additive. *Adv. Energy Mater.* **2011**, *1*, 1058−1061.
(53) Chu, T. Y.; Alem, S.; Tsang, S. W.; Tse, S. C.; Wakim, S.; Lu, J. P.; Dennler, G.; Waller, D.; Gaudiana, R.; Tao, Y. Morphology control in polycarbazole based bulk heterojunction solar cells and its impact on device performance. *Appl. Phys. Lett.* **2011**, *98*, 253301.
(54) Li, G.; Shrotriya, V.; Huang, J.; Yao, Y.; Moriarty, T.; Emery, K.; Yang, Y. High-efficiency solution processable polymer photovoltaic cells by self-organization of polymer blends. *Nat. Mater.* **2005**, *4*, 864−868.
(55) Matsuo, Y.; Sato, Y.; Niinomi, T.; Soga, I.; Tanaka, H.; Nakamura, E. Columnar structure in bulk heterojunction in solution-processable three-layered p-i-n organic photovoltaic devices using tetrabenzoporphyrin precursor and silylmethyl[60]fullerene. *J. Am. Chem. Soc.* **2009**, *131*, 16048−16050.
(56) Han, X.; Chen, X. W.; Holdcroft, S. Nanostructured morphologies and topologies of p-conjugated polymers from thermally reactive polymer blends. *Adv. Mater.* **2007**, *19*, 1697−1702.
(57) Han, X.; Chen, X. W.; Holdcroft, S. Nanostructured photovoltaic devices from thermally-reactive π-conjugated polymer blends. *Chem. Mater.* **2009**, *21*, 4631−4637.
(58) Jasieniak, J. J.; MacDonald, B. I.; Watkins, S. E.; Mulvaney, P. Solution-processed sintered nanocrystal solar cells via layer-by-layer assembly. *Nano Lett.* **2011**, *11*, 2856−2864.